Damage Tolerance of a Sandwich Panel Containing a Cracked Square Lattice Core

IGNACIO QUINTANA-ALONSO AND NORMAN A. FLECK
Cambridge University Engineering Department
Trumpington Street, Cambridge CB2 1PZ, UK

ABSTRACT: The fracture response of a sandwich panel, with a centre-cracked core made from an elastic-brittle square lattice, is explored by finite element simulations and simple analytical models. First, predictions are given for the unnotched strength of the sandwiched core and for the fracture toughness of the lattice under remote tension, remote compression or remote shear. It is assumed that the lattice fails when the local stress in the cell walls attains the tensile or compressive strength of the solid, or when local buckling occurs. Failure maps are then constructed for a cracked sandwich panel, with axes given by a dimensionless crack length and dimensionless height of the sandwich core. The shear strength of the cracked sandwich panel is examined in detail. The precise form of the failure map for shear loading depends upon the tensile failure strain of the solid and upon the relative density of the lattice. The relevance of the shear failure map to lattices made from a wide range of engineering materials is illustrated through material-property charts. An extension of the method to cyclic loading is discussed.

KEY WORDS: fracture toughness, elastic behaviour, lattice material, finite element analysis

1. INTRODUCTION

Cellular solids such as the square lattice are increasingly used in applications where severe mechanical loads and operating conditions lead to material damage. Examples include catalytic converters for automobiles, filters for liquid metal, absorbers for solar receivers, supports for space mirrors, and orthopaedic implants for bone repair. Cracks can exist in the lattice and cause a significant decrease of its fracture strength. Frequently, the lattice is loaded in a sandwich panel configuration with stiff and strong face-sheets. The damage tolerance of these structures is of concern and motivates the present work.

In this paper an investigation is given for the damage tolerance of a centre-cracked sandwich panel with an elastic-brittle square lattice core (Figure 1). The sandwich panel has rigid face-sheets and a square lattice core of cell size l, cell thickness t, and core angle 45°, as sketched in Figure 1. The panel is of height $2H$ and width $2W$, and the core contains a central crack of length $2a$. The cell walls of the lattice are adequately modelled by rigidly connected Euler beams.

* Corresponding author. Tel.: +44 1223 748240; fax: +44 1223 765046
E-mail address: naf1@cam.ac.uk

Both simple analytical models and finite element (FE) simulations are used to determine the strength of the cracked sandwich panel. Three types of loading are considered in turn: tension, compression and shear.

First, consider the case where the sandwich panel is loaded in tension by applying prescribed tensile displacements to the face-sheets. The stresses are tensile everywhere in the core, and it is assumed that failure occurs when the maximum tensile stress in the lattice attains the tensile fracture strength of the solid material σ_{TS}. Dimensional analysis tells us that the normalised net-section strength σ_{net}/σ_{TS} is a function of the four geometric non-dimensional groups: $(t/l, a/l, H/l, H/W)$. We limit attention to practical geometries where $H/W << 1$. A recent numerical study [1] of the tensile fracture response of the cracked sandwich panel, revealed two types of behaviour. A flaw-insensitive regime with no stress concentration, when $Ht/l^2 \leq 0.07$, independent of crack length. Alternatively, when $Ht/l^2 > 0.07$, the net-section strength falls below the unnotched value and is governed by the fracture toughness of the lattice.

Uniaxial compression and pure shear loading of the sandwich panel give rise to tensile and compressive stresses within the cell walls of the lattice. Consequently, the structure may fail by (i) local tensile failure, (ii) local compressive failure or by (iii) elastic buckling of the cell walls. The normalised net-section strength depends upon the geometric non-dimensional groups $t/l, a/l, H/l$; *and* upon the material groups σ_{CS}/σ_{TS}, σ_{CS}/E_S, where E_S is the Young's modulus and σ_{CS} the compressive strength of the solid. The sensitivity of the fracture strength to the above non-dimensional groups is addressed herein.

The load transfer length λ

Quintana-Alonso and Fleck [2] have shown that the material length scale $\lambda \equiv l^2/t$ plays a central role in the response of the square lattice under general loading. Load transfer into the lattice occurs over this length scale by a shear lag phenomenon [3]. For example, shear bands of length λ emanate from the tip of a mode I crack at $\phi = \pm 45^\circ$, see Figure 2.

Outline of study

First, analytical expressions are given for the unnotched strength of the sandwich panel. The buckling modes predicted for compressive loading of the sandwich structure are verified by means of a rubber lattice. Second, the fracture toughness of the lattice is calculated by the finite element method. Third, simple analytical models are proposed to explain the regimes of fracture behaviour of the cracked panel. These models are then used to construct fracture maps for the centre-cracked panel, with non-dimensional axes given in terms of the sandwich geometry. Finally, we analyse in some detail the fracture strength of the cracked panel subjected to shear loading. A fracture map is presented and validated by finite element simulations. The relevance of the map to engineering solids is explored through material-property charts.

2. UNNOTCHED STRENGTH OF THE CORE

In the absence of a crack, the strength of the sandwich geometry shown in Figure 1 is determined by classical beam theory. Expressions for the unnotched strength of the panel under remote tension, compression, and shear are listed in Table 1. The formulae take into account both stretching and bending of the cell walls, and have been validated by FE calculations [2].

For the case of remote tension, local failure within the cell walls is always tensile in nature. In contrast, for remote compression and shear, local failure can be tensile, compressive, or can be due to elastic buckling. The dominant local failure mechanism depends upon the material ratios σ_{CS}/σ_{TS}, σ_{CS}/E_S, and upon the stockiness t/l.

Compressive buckling

A preliminary finite element analysis using ABAQUS (version 6.7-1) has been performed of the buckling modes exhibited by the square lattice. In the sandwich configuration, the core is subjected to uniaxial straining and the appropriate buckling mode is shown in Figure 3a. A periodic cell calculation was conducted on a FE mesh containing 30 lattice cells in the vertical direction. The number of lattice cells in the transverse direction was varied from 1 to 100 in order to ensure that the lowest mode had been detected. In the simulations, 10 Timoshenko beam elements (type *B21* in ABAQUS) were used to model each cell wall. The observed eigenmode has the feature that each cell wall behaves as a pin-jointed Euler strut of length l. This leads to a simple analytical prediction of the buckling load, given in Table 1.

Shear buckling

An eigenvalue analysis of the shear buckling modes has also been performed using ABAQUS (version 6.7-1). The FE simulations indicate that buckling again occurs in a periodic cruciform manner, see Figure 4. Each cell wall behaves as an Euler strut of length l, but with end rotational restraint of torsional stiffness k provided by the adjoining tensile bars, see sketch in Figure 4. The buckling load is [4]

$$P_{cr} = \frac{n^2 \pi^2 E_S I}{l^2} \tag{1}$$

with $I = t^3/12$ per unit depth. The factor n describes the rotational stiffness of the joints where the cell walls meet. If rotation is freely allowed, $n = 0.5$; if no rotation is possible, $n = 2$. The unnotched shear strength for local buckling follows from equilibrium, giving

$$\tau_u^B = n^2 \frac{\pi^2}{12}\left(\frac{t}{l}\right)^3 E_S \tag{2}$$

Finite element calculations suggest $n = 1.51$. A simple direct estimate for n can be obtained. In the buckled state, the tensile bars inclined at $+45^\circ$ are subjected to alternating point torques, from one joint to the next (Figure 4). Simple beam theory for the adjoining tensile bars provides the desired torsional stiffness $k = 4E_S I/l$. Newmark [5] gives a useful approximate formula for the dependence of n in Equation (2) upon the value of k; his formula implies $n = 1.44$, which is in satisfactory agreement with the FE result of $n = 1.51$.

3. FRACTURE TOUGHNESS OF THE LATTICE

Numerical predictions of the fracture toughness of the square lattice can be obtained by solving the boundary layer problem as sketched in Figure 2. A FE mesh of size 600×600 lattice cells is constructed using Euler-Bernoulli beams. On the boundary of this model, the applied displacements $\underset{\sim}{u}$ are derived from a *K*-field in an equivalent orthotropic continuum [6].

This configuration, referred to as boundary layer analysis, simulates the near-tip conditions associated to a *K*-field. The deformation field in the orthotropic lattice is characterised by narrow zones of intense bending emanating from the crack tip along the $\pm 45^\circ$ directions (Figure 2). The length of these bands is of order $\lambda \equiv l^2/t$, and must be small relative to the size of the model ($\lambda << L$) in order for the boundary layer analysis to be valid.

Linear elastic calculations are performed for varying stockiness t/l of the lattice. The fracture toughness for local tensile failure (K_{IC}^T for mode I and K_{IIC}^T for mode II) is calculated by equating the maximum tensile stress at any point in the lattice to the tensile strength σ_{TS} of the solid. Similarly, for local compressive failure the minimum compressive stress in the lattice is equated to the compressive strength σ_{CS} of the solid to obtain K_{IC}^C and K_{IIC}^C for modes I and II respectively. Power law fits to the predicted values are given in Table 2.

An eigenvalue extraction is used in the FE calculations in order to determine the bifurcation loads for buckling. The buckling mode under mode I compression is shown in Figure 3b. The so-obtained buckling fracture toughness (Table 2) has been validated by full non-linear elastic simulations with small initial geometric imperfections [2]. In the post-buckling regime, a significant elevation of strain near the crack tip was observed, confirming the relevance of the buckling fracture toughness, K_{IC}^B and K_{IIC}^B, as a useful parameter.

Analytical models of the fracture toughness can be found in the recent literature [7, 8, 9]. These models relate the crack tip elastic fields of an equivalent continuum to the stress state within the lattice. The estimates obtained have the correct functional form and are in close agreement with the numerical predictions of Table 2.

4. EXPERIMENTAL VALIDATION OF BUCKLING MODES

In order to validate the buckling modes observed in the FE simulations (Figure 3), a rubber lattice was manufactured and tested. The model was made by pouring a degassed mixture of silicon rubber* and hardener into a mould. The mould consisted of a PMMA base along with machined steel formers (square blocks) screwed onto it at appropriate spacing to produce the desired wall thickness. The resulting lattice had a wall thickness $t = 3\,\text{mm}$ and a cell size $l = 28.4\,\text{mm}$, giving a stockiness $t/l = 0.106$. Steel face-sheets were bonded with cyanoacrylate adhesive to the rubber lattice, as depicted in Figure 5a.

Figures 5b and 5c show the deformation of the unnotched sandwich core under tension and compression, respectively. In tension, the lattice deforms by the stretching and bending of the cells walls (Figure 5b). In compression, the cell walls bend on first loading; but when a critical stress is reached the cells collapse by elastic buckling (Figure 5c). This mode is identical to that predicted in the FE simulations, see Figure 3a.

Now introduce a macroscopic crack into the lattice. The collapse mode for compressive loading is shown in Figure 5d. It is characterised by local buckling of the cell walls at the crack tip. The observed buckling mode confirms the predicted mode of Figure 3b.

5. REGIMES OF BEHAVIOUR OF THE CRACKED SANDWICH PANEL

In Sections 2 and 3 we obtained expressions for the unnotched strength of the core and the fracture toughness of the lattice. Now consider the fracture strength of the sandwich panel containing a finite centre-crack of length $2a$. In this section we describe simple analytical models in order to interpret the regimes of fracture behaviour of the cracked sandwich panel. Figure 6 illustrates the three regimes of behaviour, valid for all loading conditions. The details are as follows.

5.1 Regime I

No stress concentration exists at the crack tip. The stress state within the lattice is such that the bending component is negligible with respect to the stretching contribution. This is the damage tolerant regime: the net strength of the panel equals the unnotched strength, $\sigma_{net} = \sigma_u$ and $\tau_{net} = \tau_u$ (see Table 1).

A sketch of the stress state within the sandwich core for Regime I is shown in Figure 6a. Long elastic shear bands of high bending stresses develop at $\pm 45^\circ$ from the crack tip. The length of the bands is limited by the height of the panel.

5.2 Regime II

* Silcoset 105 *(acc silicones)*

The crack is sufficiently long compared to the height of the sandwich panel that the core behaves as an orthotropic elastic strip with a semi-infinite crack, see Figure 6b. Upstream of the crack tip, the lattice is in a biaxial state of stress, whereas downstream it is unloaded. At the crack tip a *K*-field exists, and the length λ of the shear bands is small relative to the height of the panel, $\lambda << H$. The stress intensity factors are given by

$$K_I = F_I \sigma_{net} \sqrt{H} \tag{3}$$

for mode I, and by

$$K_{II} = F_{II} \tau_{net} \sqrt{H} \tag{4}$$

for mode II, where the calibration functions are $F_I = F_{II} = 2^{3/4} \left(t/l\right)^{1/2}$, see reference [1]. Failure initiates when the stress intensity factor K_I attains the critical value K_{IC}, or when K_{II} attains K_{IIC}.

5.3 Regime III

The crack is much smaller than the height and width of the sandwich panel, see Figure 6c. The *K*-calibration for an orthotropic panel containing a short central crack of length $2a$ applies and is approximately given by

$$K_I = \sigma_{net} \sqrt{\pi a} \tag{5}$$

for mode I, and

$$K_{II} = \tau_{net} \sqrt{\pi a} \tag{6}$$

for mode II, as reported in [1]. Upon equating K_I to K_{IC}, or K_{II} to K_{IIC}, we obtain the net strength of the cracked sandwich panel for Regime III.

6. FRACTURE MAPS

The above analytical models can be used to construct fracture maps with axes written in terms of the sandwich geometry. The net-section strength equals the unnotched strength in Regime I, depends upon l^2/Ht in Regime II, and depends upon l/a in Regime III. Consequently, we construct a fracture map with axes (a/l, Ht/l^2), as shown in Figure 7 for uniaxial tension.

The boundaries between regimes are obtained by equating the expressions for the strength within each regime. The boundary between Regimes II and III is given by $Ht/l^2 = 1.1 a/l$, for all types of loading. A physical constraint on the minimum crack length, $a/l \geq \sqrt{2}$, is also imposed on the map. In uniaxial tension, the boundary between Regimes I and II is given by $Ht/l^2 = 0.07$, see Figure 7. In uniaxial compression, however, this boundary depends upon the local failure mechanism. Its location is dictated by the values of the non-dimensional groups

σ_{CS}/σ_{TS} and $l^2\sigma_{TS}/\left(t^2E_S\right)$ [2]. In shear, the boundary is set by the value of $l^2\sigma_{TS}/\left(t^2E_S\right)$, as we shall see in the following section.

It is straightforward to add contours of strength to the map, using the expressions of Tables 1 and 2, and Equations (3)-(6). The maps are universal for all values of bar stockiness, but they are limited to the practical regime where W/H is large.

The compressive response of the cracked sandwich panel is similar to the shear response discussed in the following section. Fracture maps analogous to Figure 7 are obtained from the predictions of unnotched strength and crack-closing fracture toughness presented in Tables 1 and 2. A full account of the cracked sandwich panel subjected to compression is given in [2].

7. SHEAR LOADING OF THE CRACKED SANDWICH PANEL

The core of a sandwich panel is primarily designed to resist shear loads. In this section, we examine the failure mechanisms of a cracked sandwich panel subjected to shear. The shear fracture map is given and is validated by a series of FE simulations. The relevance of the fracture map to engineering solids is illustrated through material-property charts. Then, the analysis is extended to the fatigue strength of lattices.

The mode II fracture toughness K_{IIC} of the square lattice equals $\min\left(K_{IIC}^C, K_{IIC}^T, K_{IIC}^B\right)$. It depends upon the lattice geometry and upon the cell wall properties. Likewise, the unnotched shear strength τ_u of the sandwich panel equals $\min\left(\tau_u^C, \tau_u^T, \tau_u^B\right)$. We limit attention to solids which satisfy $\sigma_{CS}/\sigma_{TS} > 1$, so that compressive local failure of the unnotched lattice and of the cracked lattice never occur. This is not a severe restriction on material choice: almost all engineering solids have the characteristic that $\sigma_{CS}/\sigma_{TS} > 1$.

Note from Table 1 that the unnotched strength is buckling-governed when $\tau_u^B/\tau_u^T \equiv 1.88t^2E_S/\left(l^2\sigma_{TS}\right) < 1$. Similarly, from Table 2, the fracture toughness is buckling-governed when $K_{IIC}^B/K_{IIC}^T \equiv 6.25t^2E_S/\left(l^2\sigma_{TS}\right) < 1$. Thus, the value of the single non-dimensional group

$$\Pi \equiv \frac{\sigma_{TS}}{E_S}\left(\frac{l}{t}\right)^2 \tag{7}$$

dictates whether the unnotched strength and the fracture toughness are due to buckling or tensile local failure. This competition of local failure criteria is summarised in Table 3.

Now consider the fracture strength of the sandwich panel containing a finite centre-crack of length $2a$, for any given value of Π. The failure map for the cracked sandwich panel subjected to prescribed shear displacements is given in

Figure 8. The three distinct regimes of behaviour are identified. In Regime I, the stress state is uniform throughout the core and the net-section strength equals the unnotched strength. In Regimes II and III, linear elastic fracture mechanics (LEFM) applies and the net-section strength is dictated by the fracture toughness of the lattice.

The boundaries of the shear map follow immediately from equating τ_{net} in neighbouring regimes. The boundary between Regimes I and II is given by

$$\left(\frac{Ht}{l^2}\right)_{trans} = \frac{1}{2\sqrt{2}}\frac{1}{l}\left(\frac{K_{IIC}}{\tau_u}\right)^2 \tag{8}$$

for all Π.

We emphasise that the expressions in Tables 1 and 2 for τ_u and K_{IIC} depend upon the active failure mechanisms, as dictated by the value of Π. Recall that the competition between cell wall buckling and local tensile failure is determined by the value of Π, as summarised in Table 3. Π scales with the material index σ_{TS}/E_s and with $(l/t)^2$. Thus, the transition value of Ht/l^2 between Regimes I and II is dependent upon material choice: in Figure 8 it is shown for the extreme values $\Pi = 1.88$, $\Pi = 6.25$, and for the intermediate choice $\Pi = 3.5$. The boundary between Regimes II and III is given by $Ht/l^2 = 1.1a/l$, for all Π.

Note that the case of τ_u determined by local tensile failure of the lattice struts and K_{IIC} by local buckling is not viable. This is because for τ_u to be tensile-governed $\Pi < 1.88$, while for K_{IIC} to be buckling-governed $\Pi > 6.25$.

This map is analogous to that for given in Figure 7 for uniaxial tension of the sandwich panel. In uniaxial tension, however, the boundary between Regimes I and II is fixed at $Ht/l^2 = 0.07$, due to the fact that for remote tension, local failure within the cell walls is always tensile in nature. The map is universal for all values of strut stockiness, but it is limited to the practical geometries where W/H is large.

7.1 Verification of the Fracture Map for Shear Loading

Selected linear elastic FE calculations have been performed to validate the above analytical predictions. First limit attention to the parameter regime where local tensile failure dominates over buckling, $\Pi \le 1.88$, and so do not consider buckling. A FE model of the cracked sandwich core was created using Euler-Bernoulli beam elements. The model had fixed aspect ratios $H/l = 70\sqrt{2} \approx 100$ and $H/W = 1/20$. The crack was introduced by splitting the joints along the cracking plane, but keeping intact the struts on either face of the crack, as sketched in the inset of Figure 1. Shear loading was imposed by prescribing the horizontal displacement of the lattice joints attached to the face-sheets, with

rotational constraint of the nodes. We investigate the sensitivity of the shear strength of the sandwich panel to crack length a/l and stockiness t/l, as follows.

The sensitivity of the net-section strength to crack length is shown in Figure 9. We note from Table 1 that the unnotched strength for local tensile failure is approximately $\tau_u^T \approx \sigma_{TS}\, t/l$ when t/l is small, and so the net shear strength τ_{net} has been normalised by $\sigma_{TS}\, t/l$ in Figure 9, such that

$$\overline{\tau} \equiv \frac{\tau_{net}}{\sigma_{TS}} \frac{l}{t} \tag{9}$$

Analytical predictions are included (solid lines). Close agreement between the analytical formulae and the numerical predictions is observed in all three regimes.

The sensitivity of the net-section strength to Ht/l^2 is examined in Figure 10 for a fixed crack length $a/l = 3\sqrt{2}$. At small Ht/l^2 Regime I exists and $\tau_{net} = \tau_u$. With increasing Ht/l^2 the response becomes toughness-controlled and the net-strength falls below the unnotched value: in Regime II the values of τ_{net} are given by Equation (4), and in Regime III by Equation (6), upon making use of the appropriate fracture toughness K_{IIC}^T listed in Table 2.

Additional FE checks on the buckling strength of the centre-cracked sandwich panel have been conducted by an eigenvalue analysis. The FE results are shown in Figure 11 for two extreme values of crack length: $a/l = 5\sqrt{2}$ and $a/l = 350\sqrt{2}$. The bifurcation stress τ_{net}^B normalised by the buckling shear strength of the unnotched core τ_u^B is plotted against Ht/l^2. The FE data are well predicted by the simple analytical models, corroborating the applicability of the buckling fracture toughness K_{IIC}^B as a useful fracture parameter.

7.2 Strategy for Determining of the Shear Strength of a Centre-Cracked Lattice Core

For a given sandwich geometry and a given core material, the shear strength of a centre-cracked lattice core is determined as follows.

Step 1:
Calculate $\Pi \equiv \sigma_{TS} l^2 / E_S t^2$ to determine the active local failure mechanism dictating the value of τ_u and K_{IIC}, see Table 3. The values of unnotched shear strength τ_u and mode II fracture toughness K_{IIC} are then calculated from Tables 1 and 2, respectively.

Step 2:
Identify whether Regime II or III is potentially active:

$a/l > Ht/l^2$ Regime II

$a/l < Ht/l^2$ Regime III

For the potentially active regime, and knowing K_{IIC}, calculate the value of $\tau_2 = \tau_{net}$, as given by Equation (4) or Equation (6).

Step 3:

The critical shear strength of the centre-cracked lattice core is taken as $\tau_{cr} = \min(\tau_u, \tau_2)$.

7.3 Application to Engineering Solids

A material-property chart is now presented to show the active failure mechanisms for a wide range of engineering materials when manufactured into a lattice core and loaded in shear. The active mechanisms are presented for both the unnotched shear strength τ_u of the lattice core and for the mode II fracture toughness K_{IIC}.

Recall that the competition between cell wall buckling and local tensile failure is dictated by the value of Π, as summarised in Table 3. Π scales with the material index σ_{TS}/E_S and with $(l/t)^2$. Thus, the value of Π is dependent upon material choice, for any given t/l.

This competition of local failure criteria is explored through a material-property chart in Figure 12. Plots of the tensile strength σ_{TS} versus the Young's modulus E_S have been generated for engineering materials using the CES [10] software (Figure 12). We limit materials to those which are elastic-brittle. Data for a given class of materials (e.g. technical ceramics) are enclosed in property-envelopes.

For the unnotched strength (dotted lines in Figure 12), the contour $\Pi = 1.88$ marks the transition from local buckling to local tensile failure. Likewise, for the fracture toughness (dash-dot in Figure 12), the contour of $\Pi = 6.25$ delimits this transition. These boundaries have been added to the charts for selected values of t/l.

For stocky lattices with $t/l = 0.1$, almost all materials possess a value of Π which is much less than 1.88 (they lie to the right of the transition boundaries). Consequently, the unnotched strength and the fracture toughness are governed by local tensile failure. In contrast, for more slender lattices, $t/l = 0.01$, the lines of constant $\Pi = 1.88$ and 6.25 cut through the body of the data: there is an active competition between buckling and local tensile failure of the cell walls, and the dominant failure mechanism is material-dependent. We conclude that for the same material, the local failure mechanism may be different in an unnotched lattice core than in a cracked one. For example, a glassy lattice core of $t/l = 0.01$ possesses a value of Π between 1.88 and 6.25 (see Figure 12). Hence, it would collapse by local buckling in an unnotched strength test, but it would fail by the attainment of the tensile strength of the cell wall material in a fracture toughness test.

The current study is also of relevance to the fatigue strength of *metallic lattices*. Following Gibson and Ashby [7] and Huang and Lin [11] we argue that fatigue failure of the cracked lattice is due to cyclic failure of the most heavily loaded strut. Now limit attention to the fatigue limit of the lattice. At infinite fatigue life, this critical strut is subjected to local stress of amplitude equal to the endurance limit σ_e of the solid.

The map shown in Figure 8 can be re-interpreted as a fatigue fracture map to describe the fatigue strength of lattice materials, with the following modification. Replace the tensile strength σ_{TS} by the amplitude of fatigue loading σ_e of the solid at the endurance limit (10^7 cycles). Also, replace τ_{net} by the amplitude of fatigue loading τ_a at the endurance limit for the cracked sandwich panel. Then, the unnotched fatigue strength of the lattice is given by

$$\tau_u^T = \frac{t/l}{1+3/2\left(t/l\right)}\sigma_e \tag{10}$$

and the mode II fatigue threshold for the metallic lattice is given by

$$\left(\Delta K_{II}^T\right)_{th} = 0.88\left(t/l\right)\sigma_e\sqrt{l} \tag{11}$$

in accordance with the equations listed in Tables 1 and 2. Buckling remains a possibility under cyclic loading and the expressions for $\left(\tau_u^B, K_{IIC}^B\right)$ still hold. Equations (4) and (6) apply, but with the substitution $\left(\sigma_{TS}, \tau_{net}\right) \to \left(\sigma_e, \tau_a\right)$ for cyclic loading.

The ratio of endurance strength to tensile strength σ_e/σ_{TS} is termed the fatigue ratio. It is of the order of $0.35-0.5$ for metallic alloys, and is close to unity for ceramics. For any given solid and stockiness of lattice, the value of Π for cyclic loading is less than that for monotonic loading by a factor equal to the fatigue ratio.

It is straightforward to generate a fatigue chart of engineering materials again using CES [10], with the endurance limit σ_e as the y-axis and the Young's modulus E_S as the x-axis (Figure 13). Lines of $\Pi = 1.88$ and 6.25 are included for $t/l = 0.01$ and 0.1. We have included all engineering materials in the fatigue property chart of Figure 13 in view of the fact that the cyclic stress state is given by the elastic solution at the endurance limit. Thus, in the fatigue case, our elastic-brittle analysis is not restricted to solids of low ductility. It is clear from Figure 13 that materials exist which undergo cell wall buckling at the endurance limit for both small $t/l = 0.01$ and large $t/l = 0.1$. These materials include elastomers, polymers and foams. Most metallic alloys undergo fatigue failure at the cell-wall level for $t/l = 0.1$, but buckle at $t/l = 0.01$.

No experimental data have been found in the literature to support or refute Equation (11). Formulae similar to (11) have been developed for open-cell

metallic foams and polymeric foams, see [7, 12, 13]. These experimental and theoretical studies support the idea that the fatigue crack growth threshold $\left(\Delta K_{II}^{T}\right)_{th}$ is dependent upon the cyclic fatigue strength σ_e of the cell wall, and upon the cell size l.

8. CONCLUDING REMARKS

It is recognised that brittle solids exhibit a scatter of failure strength: variable flaw sizes and a random orientation within the brittle cell walls lead to variations in the tensile strength of the solid material σ_{TS}. Statistical variations in the cell wall strength are usually quantified by assuming a Weibull distribution. The effect of specimen geometry and Weibull modulus m upon the fracture map can then be explored. It is expected that the larger the sandwich panel the more likely it is to be strength-controlled, for a given cell size of the lattice. Also, the domains of toughness-controlled fracture will shrink as the Weibull modulus is decreased. This is not explored further here, but is discussed for the tensile loading of a cracked sandwich panel in [1].

Microstructural imperfections such as wavy struts and displaced joints are expected to have a knock-down effect upon the fracture properties of elastic-brittle lattices. The sensitivity of fracture toughness to imperfections in the form of displaced joints has been explored by Romijn and Fleck [9]. Their analysis indicates that the fracture toughness of the square topology is imperfection-sensitive. Their results can be used to modify the strength predictions of the cracked sandwich panel with imperfections present at the cell wall level.

9. REFERENCES

1. Quintana-Alonso, I. and Fleck, N.A. (2007). The Damage Tolerance of a Sandwich Panel Containing a Cracked Honeycomb Core, *Journal of Applied Mechanics*. In press.

2. Quintana-Alonso, I. and Fleck, N.A. (2008). The Compressive Response of a Sandwich Panel with a Cracked Honeycomb Core. Submitted to *Journal of Mechanics and Physics of Solids.*.

3. Wicks, N. and Guest, S.D. (2004). Single Member Actuation in Large Repetitive Truss Structures, *International Journal of Solids and Structures*, **41**(3-4): 965-978.

4. Timoshenko, S.P. and Gere, J.M. (1961). *Theory of Elastic Stability*, 2nd ed. McGraw-Hill, New York.

5. Newmark, N.M. (1949). A Simple Approximate Formula for Effective End-Fixity of Columns, *Journal of the Aeronautical Sciences*, **16**: 116.

6. Sih, G.C., Paris, P.C. and Irwin, G.R. (1965). On Cracks in Rectilinearly Anisotropic Bodies, *International Journal of Fracture Mechanics*, **1**(13): 189-203.

7. Gibson, L.J. and Ashby, M.F. (1999). *Cellular Solids: Structure and Properties*, 2nd ed., Pergamon Press, Oxford, UK.

8. Quintana Alonso, I. and Fleck, N.A., (2007). Damage Tolerance of an Elastic-Brittle Diamond-Celled Honeycomb, *Scripta Materialia*., **56**(8): 693-696.

9. Romijn, N.E.R. and Fleck, N.A. (2007) The Fracture Toughness of Planar Lattices: Imperfection Sensitivity, *Journal of Mechanics and Physics of Solids*, **55**(12): 2538-2564.

10. CES EduPack 2007, The Cambridge Engineering Selector, Granta Design, Rustat House, 62 Clifton Road, Cambridge CB1 7EG, UK.

11. Huang, J.S. and Lin, J.Y. (1996) Fatigue of Cellular Materials, *Acta Mater*. **44**(1): 289-296.

12. Olurin, O.B., McCullough, K.Y.G., Fleck, N.A. and Ashby, M.F. (2001) Fatigue Crack Propagation in Aluminium Alloy Foams, *Int. J. Fatigue* **23**(5): 375-382.

13. Burman, M. and Zenkert, D. (1997) Fatigue of Foam Core Sandwich Beams, *Int. J. Fatigue* **19**(7): 551-578.

Loading	*Failure Criterion*	*Unnotched Strength*
Tension	Tensile	$\sigma_u = \frac{t/l}{1+3t/l}\sigma_{TS}$
Compression	Compressive	$\sigma_u^C = \frac{t/l}{1+3t/l}\sigma_{CS}$
	Tensile	-
	Buckling	$\sigma_u^B = 0.82(t/l)^3 E_S$
Shear	Compressive	$\tau_u^C = \frac{t/l}{1+3t/2l}\sigma_{CS}$
	Tensile	$\tau_u^T = \frac{t/l}{1+3t/2l}\sigma_{TS}$
	Buckling	$\tau_u^B = 1.88(t/l)^3 E_S$

Table 1. Unnotched strength of the $\pm 45^\circ$ square core. The superscripts T, C, and B denote the relevant local failure criterion: tensile, compressive, and buckling, respectively

Mode	*Failure Criterion*	*Fracture Toughness*
Mode I Crack opening	Tensile	$K_{IC} = 0.44(t/l)\sigma_{TS}\sqrt{l}$
Mode I Crack closing	Compressive	$K_{IC}^C = 0.44(t/l)\sigma_{CS}\sqrt{l}$
	Tensile	$K_{IC}^T = 0.74(t/l)\sigma_{TS}\sqrt{l}$
	Buckling	$K_{IC}^B = 2(t/l)^3 E_S\sqrt{l}$
Mode II	Compressive	$K_{IIC}^C = 0.44(t/l)\sigma_{CS}\sqrt{l}$
	Tensile	$K_{IIC}^T = 0.44(t/l)\sigma_{TS}\sqrt{l}$
	Buckling	$K_{IIC}^B = 2.75(t/l)^3 E_S\sqrt{l}$

Table 2. Fracture toughness of the $\pm 45^\circ$ square lattice. The superscripts T, C, and B denote the relevant local failure criterion: tensile, compressive, and buckling, respectively.

$\Pi \equiv \sigma_{TS} l^2 / E_S t^2$	τ_u	K_{IIC}	$\left(Ht/l^2\right)_{trans}$
<1.88	Tensile	Tensile	0.07
$\times$	Tensile	Buckling	Not viable
$1.88-6.25$	Buckling	Tensile	$0.02\ \Pi^2$
>6.25	Buckling	Buckling	0.76

Table 3. Competition of local failure criteria for shear loading of a cracked sandwich panel. Unnotched strength τ_u and mode II fracture toughness K_{IIC} are controlled by local cell-wall buckling or by local tensile failure. The weakest mode of local failure is dictated by the value of Π. The transition Ht/l^2 between Regimes I and II is also set by Π.

FIGURE CAPTIONS

Figure 1. Sandwich panel comprising a cracked square lattice core.

Figure 2. The finite element mesh used in the fracture toughness predictions. The crack tip is at the centre of the mesh. Shear bands form at $\phi = \pm 45^\circ$.

Figure 3. Deformed FE meshes of the buckled state in (a) an unnotched lattice, and (b) a cracked sandwich panel, under uniaxial compression.

Figure 4. Buckling of an unnotched panel subjected to remote shear. The face-sheets are allowed to displace in the x_2-direction, but rotation is not permitted. The boundary conditions on the left (L) and right (R) edges of the specimen are: $u_1^L = u_1^R$; $u_2^L = u_2^R$; $\theta^L = \theta^R$.

Figure 5. Deformation mechanisms: (a) undeformed rubber lattice with square cells attached to steel face-sheets, (b) under remote tension the cell walls stretch and bend, (c) under remote compressive loading, the cell walls buckle, (d) elastic buckling around the tip of a macroscopic crack. Cell size $l = 28.4\,\text{mm}$, wall thickness $t = 3\,\text{mm}$.

Figure 6. (a) Regime I: uniform stress with practically no stress concentration at the crack tip. (b) Regime II: *K*-field exists and strength is independent of crack length. (c) Regime III: *K*-field exists and strength scales with crack length as $a^{-1/2}$. In all three regimes, the effective stress far ahead of the crack tip is equi-biaxial and of magnitude σ_{net}.

Figure 7. Fracture map for a sandwich panel containing a central crack and subjected to *uniaxial tension*. Valid for small H/W.

Figure 8. Fracture map for a sandwich panel containing a centre crack and subjected to prescribed *shear displacements*. Map valid for small H/W .

Figure 9. Normalised shear strength as a function of crack size. Solid lines denote analytic predictions. $W/H = 20$ and $H/l = 70\sqrt{2} \approx 100$.

Figure 10. Normalised shear strength as a function of Ht/l^2 , for a sandwich panel containing a central crack of length $a/l = 3\sqrt{2}$. $W/H = 20$ and $H/l = 70\sqrt{2} \approx 100$.

Figure 11. Buckling shear strength of a cracked core. $W/H = 20$ and $H/l = 70\sqrt{2} \approx 100$.

Figure 12. Material-property chart for failure mechanisms dictating the unnotched shear strength of lattice core and the mode II fracture toughness of the $\pm 45^\circ$ square lattice.

Figure 13. Material-property chart for failure mechanisms dictating the fracture toughness and unnotched strength of a lattice core subjected to shear cyclic loading. Note that $\Pi \equiv \sigma_e l^2 / E_S t^2$.

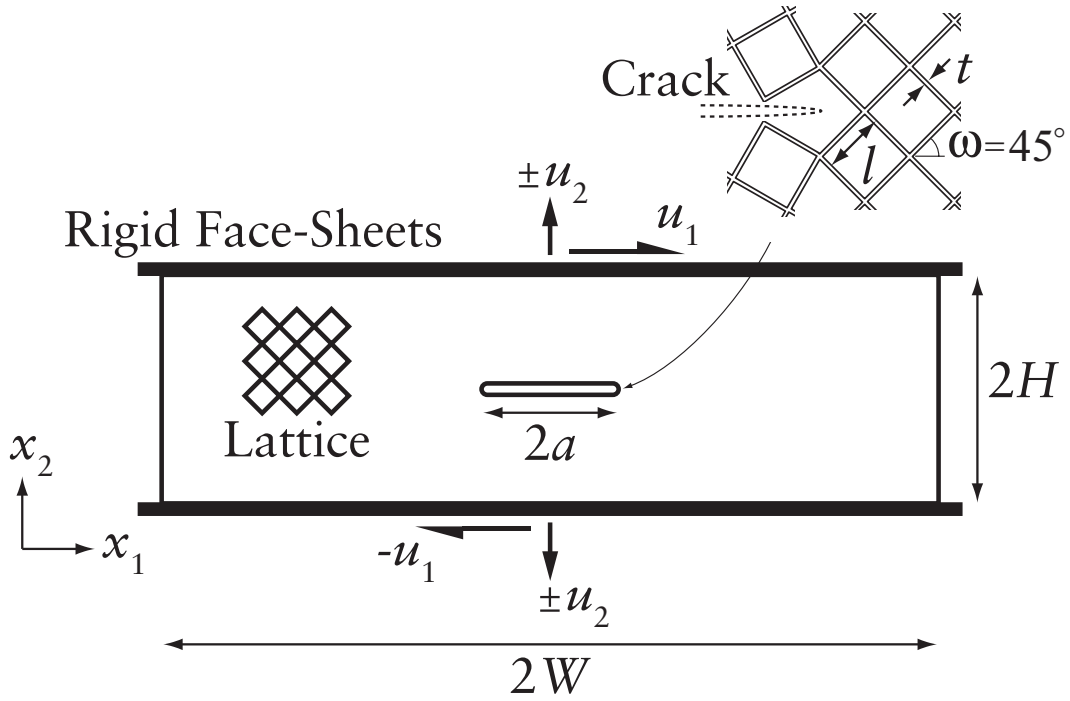

Figure 1. Sandwich panel comprising a cracked square lattice core.

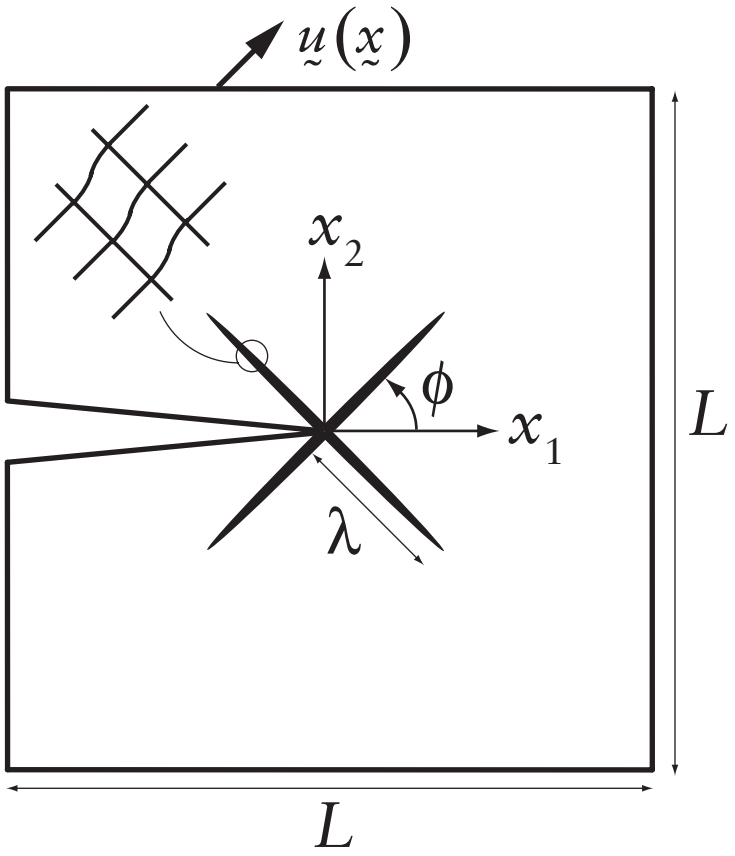

Figure 2. The finite element mesh used in the fracture toughness predictions. The crack tip is at the centre of the mesh. Shear bands form at $\phi = \pm 45^{\circ}$.

* Corresponding author. Tel.: +44 1223 748240; fax: +44 1223 765046
E-mail address: naf1@cam.ac.uk

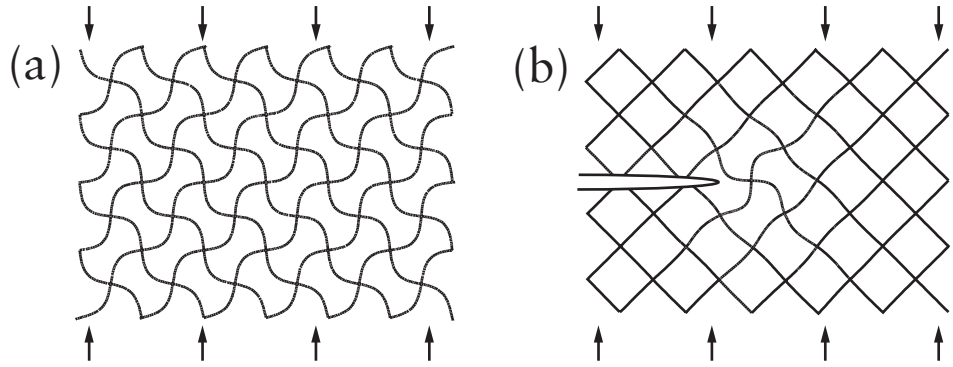

Figure 3. Deformed FE meshes of the buckled state in (a) an unnotched lattice, and (b) a cracked sandwich panel, under uniaxial compression.

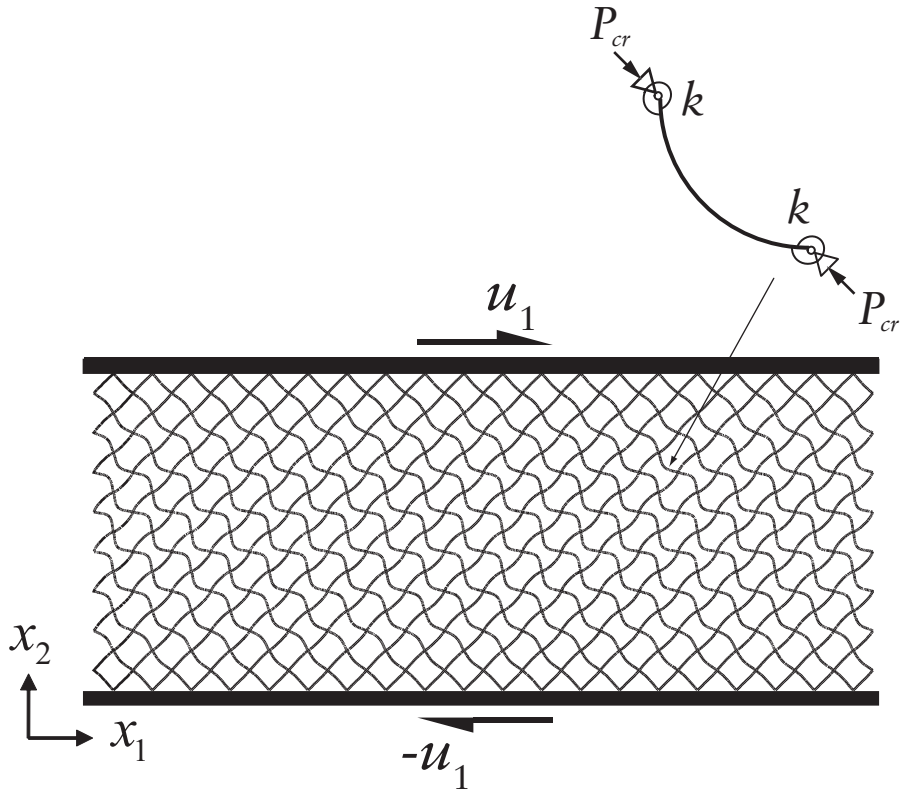

Figure 4. Buckling of an unnotched panel subjected to remote shear. The face-sheets are allowed to displace in the x_2-direction, but rotation is not permitted. The boundary conditions on the left (L) and right (R) edges of the specimen are: $u_1^L = u_1^R$; $u_2^L = u_2^R$; $\theta^L = \theta^R$.

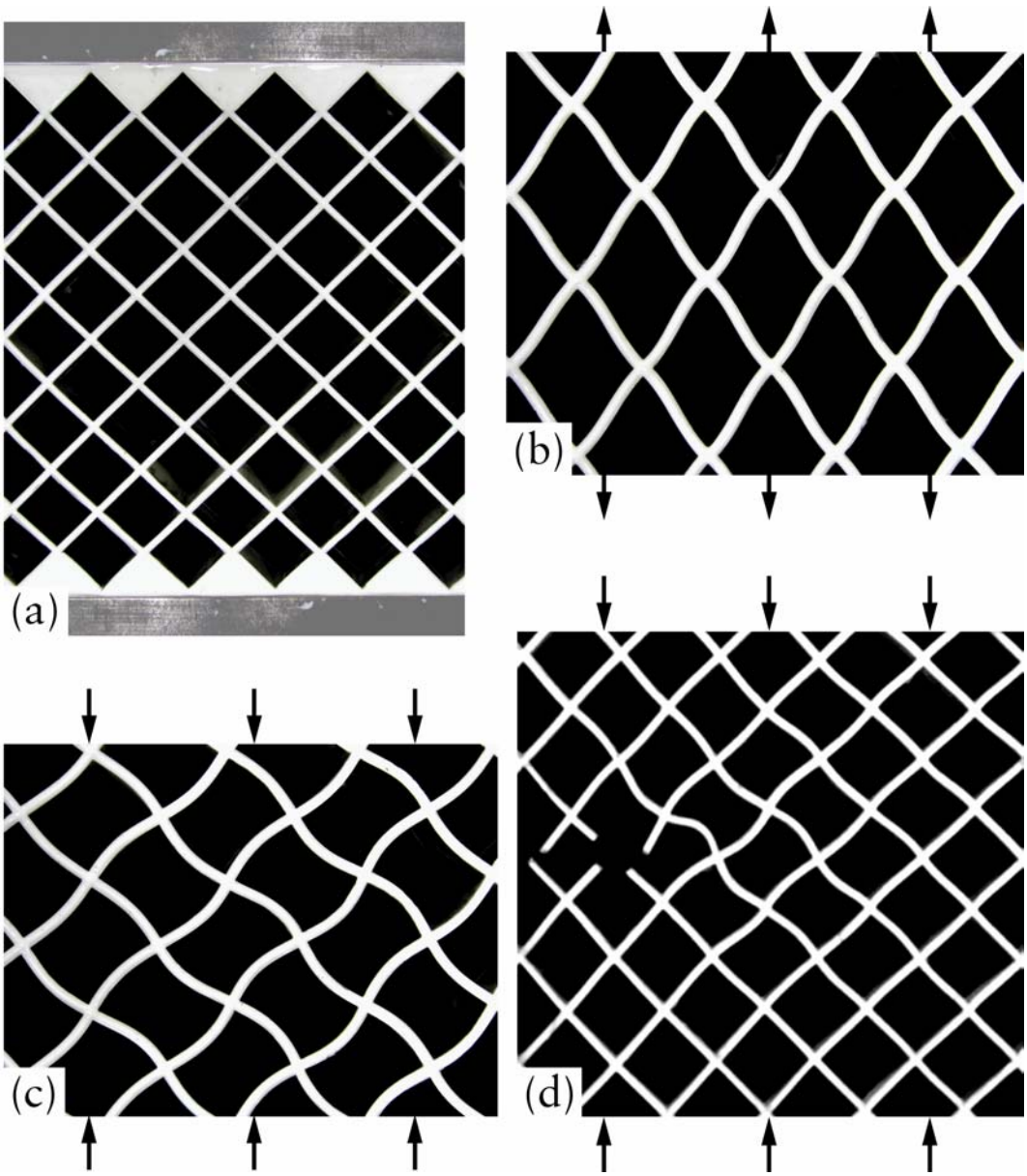

Figure 5. Deformation mechanisms: (a) undeformed rubber lattice with square cells attached to steel face-sheets, (b) under remote tension the cell walls stretch and bend, (c) under remote compressive loading, the cell walls buckle, (d) elastic buckling around the tip of a macroscopic crack. Cell size $l = 28.4\,\text{mm}$, wall thickness $t = 3\,\text{mm}$.

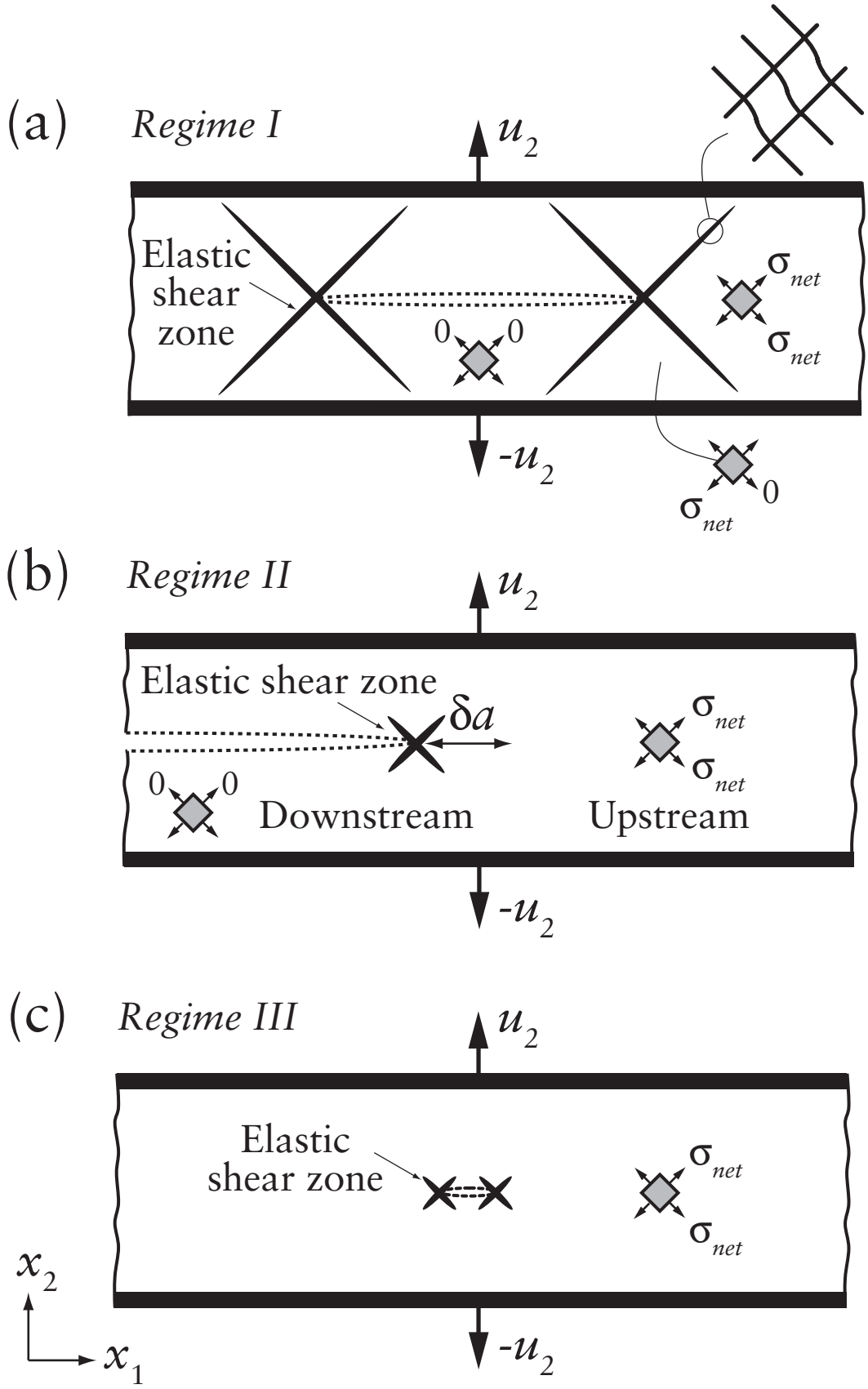

Figure 6. (a) Regime I: uniform stress with practically no stress concentration at the crack tip. (b) Regime II: *K*-field exists and strength is independent of crack length. (c) Regime III: *K*-field exists and strength scales with crack length as

$a^{-1/2}$. In all three regimes, the effective stress far ahead of the crack tip is equi-biaxial and of magnitude σ_{net}.

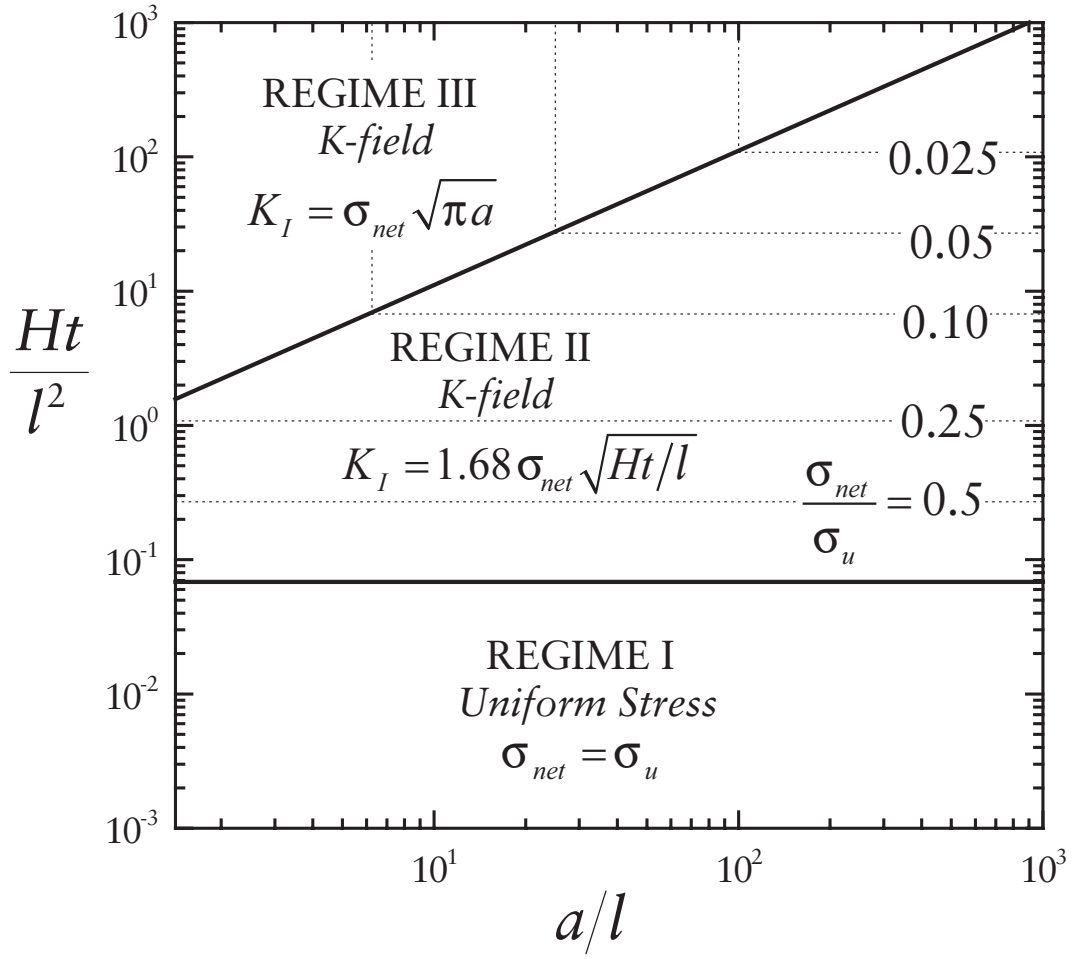

Figure 7. Fracture map for a sandwich panel containing a central crack and subjected to *uniaxial tension*. Valid for small H/W.

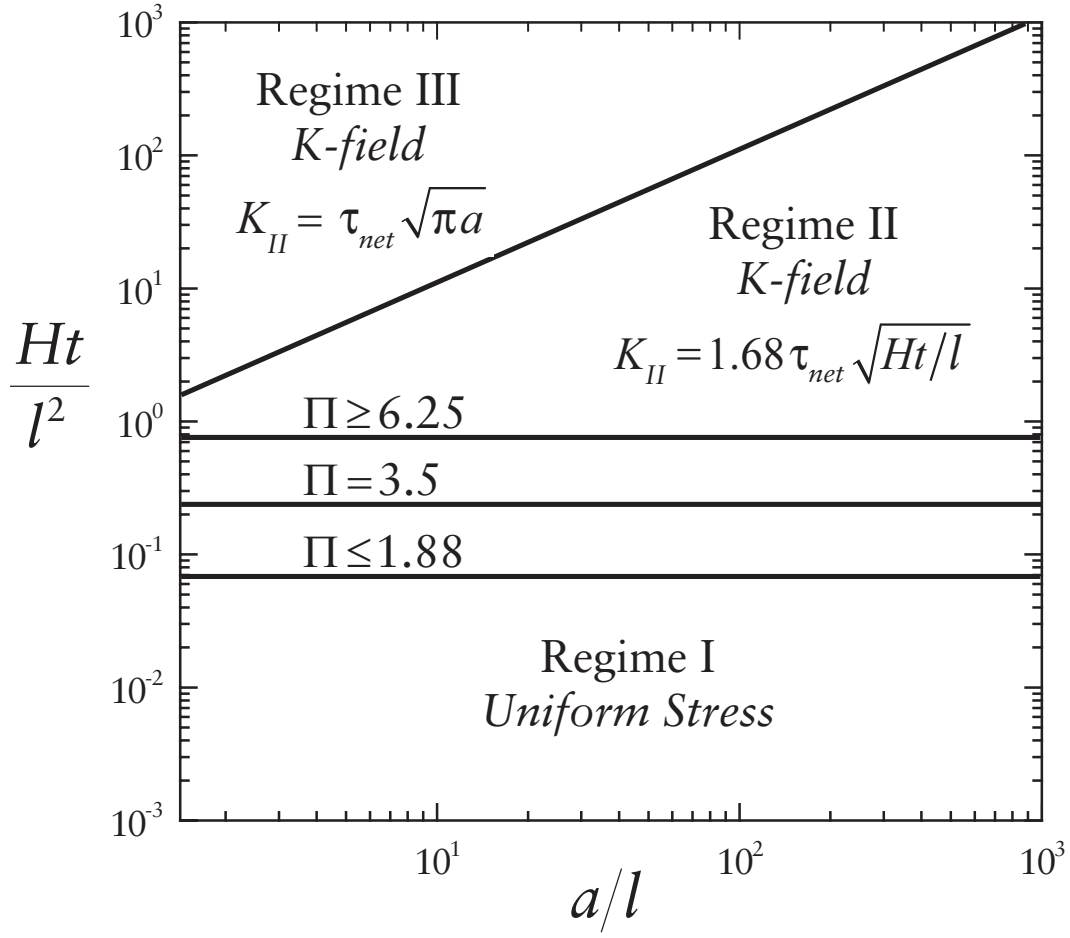

Figure 8. Fracture map for a sandwich panel containing a centre crack and subjected to prescribed *shear displacements*. Map valid for small H/W .

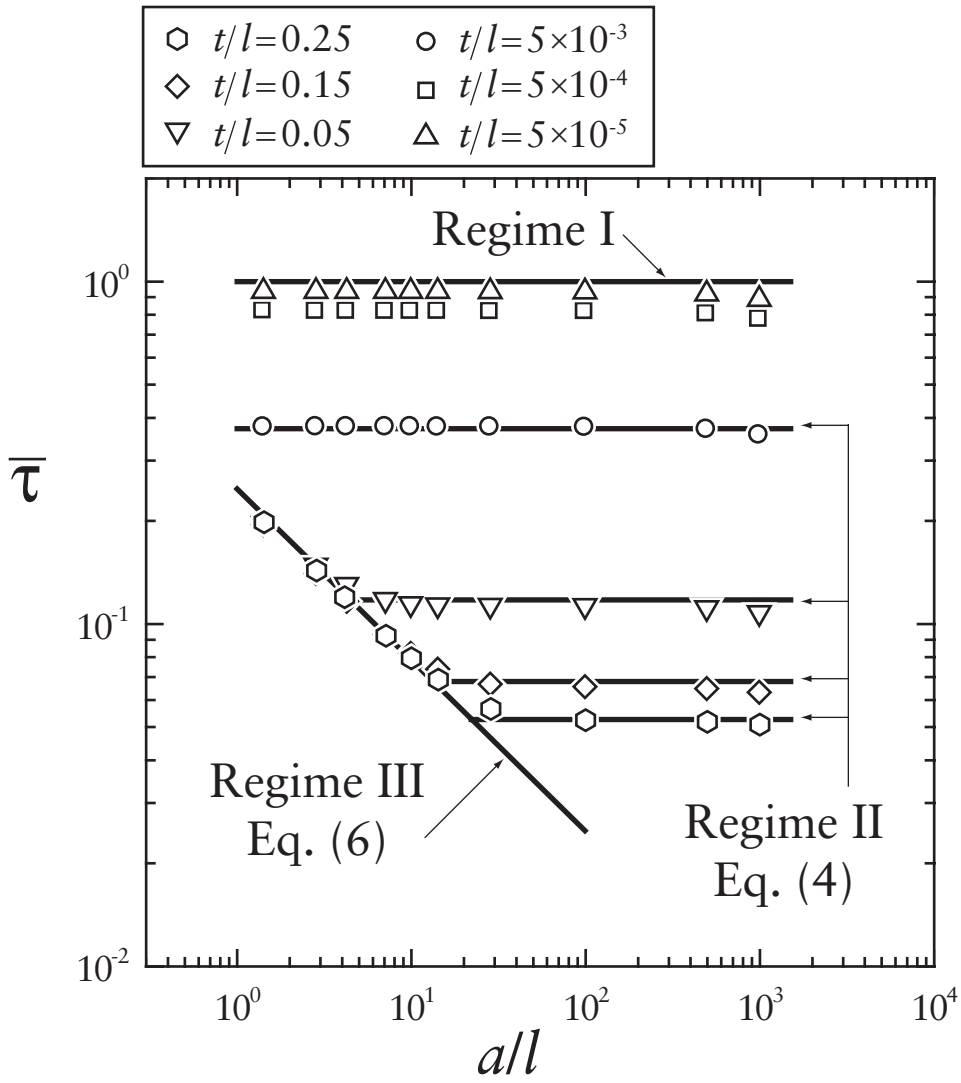

Figure 9. Normalised shear strength as a function of crack size. Solid lines denote analytic predictions. $W/H = 20$ and $H/l = 70\sqrt{2} \approx 100$.

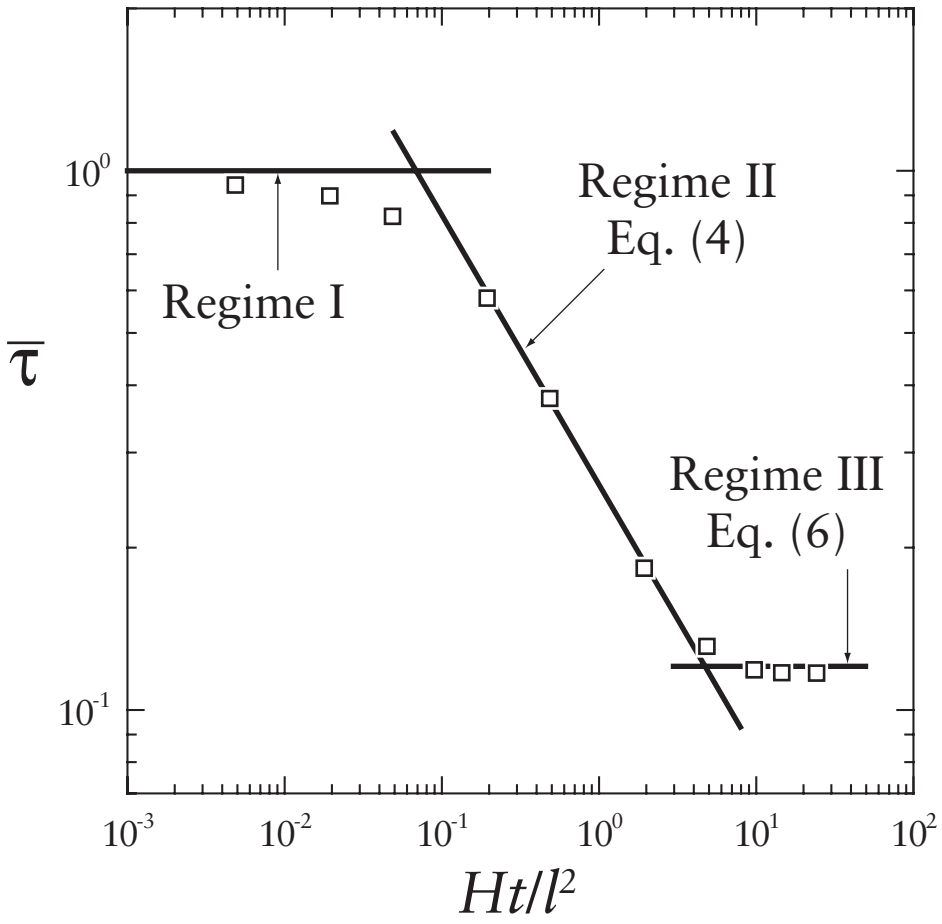

Figure 10. Normalised shear strength as a function of Ht/l^2 , for a sandwich panel containing a central crack of length $a/l = 3\sqrt{2}$. $W/H = 20$ and $H/l = 70\sqrt{2} \approx 100$.

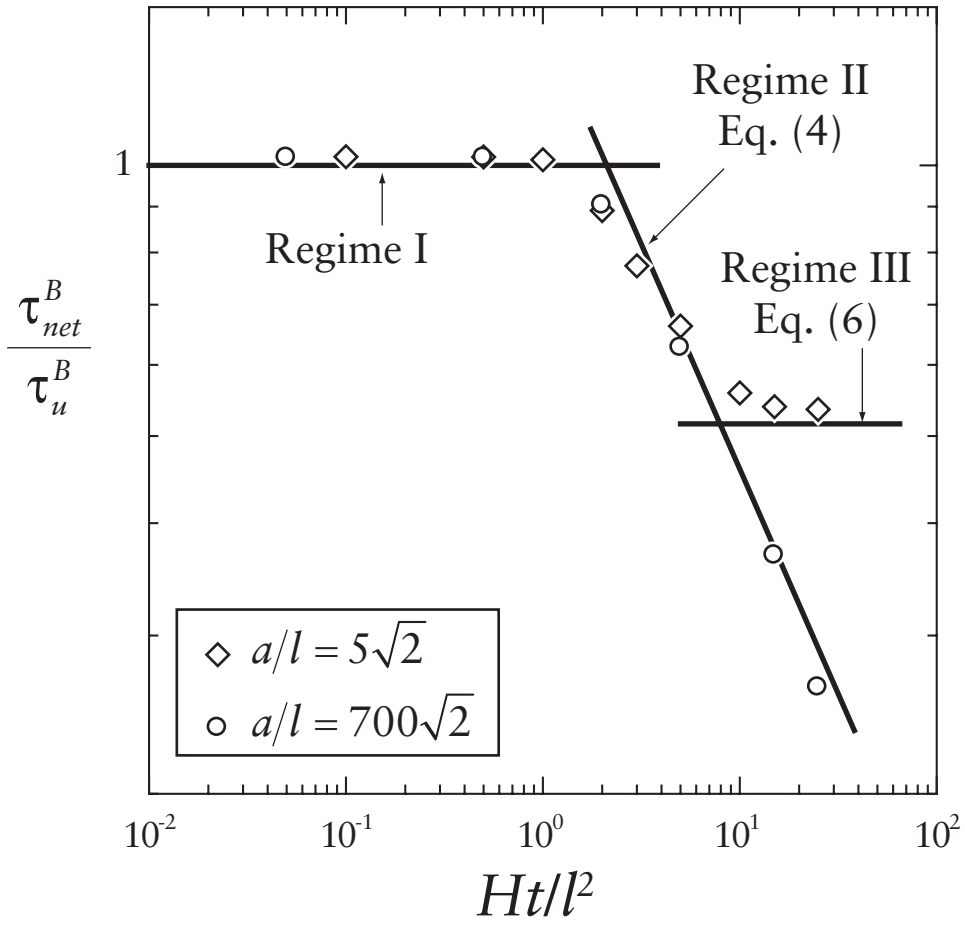

Figure 11. Buckling shear strength of a cracked core. $W/H = 20$ and $H/l = 70\sqrt{2} \approx 100$.

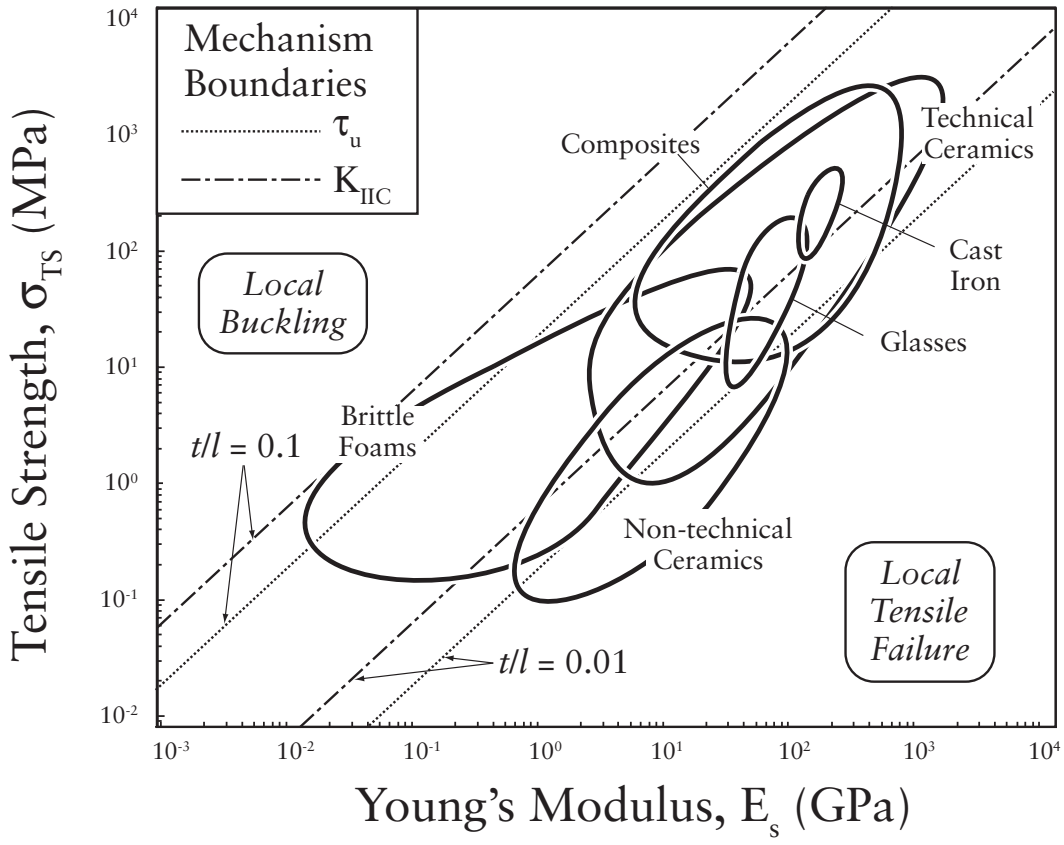

Figure 12. Material-property chart for failure mechanisms dictating the unnotched shear strength of lattice core and the mode II fracture toughness of the $\pm 45^{\circ}$ square lattice.

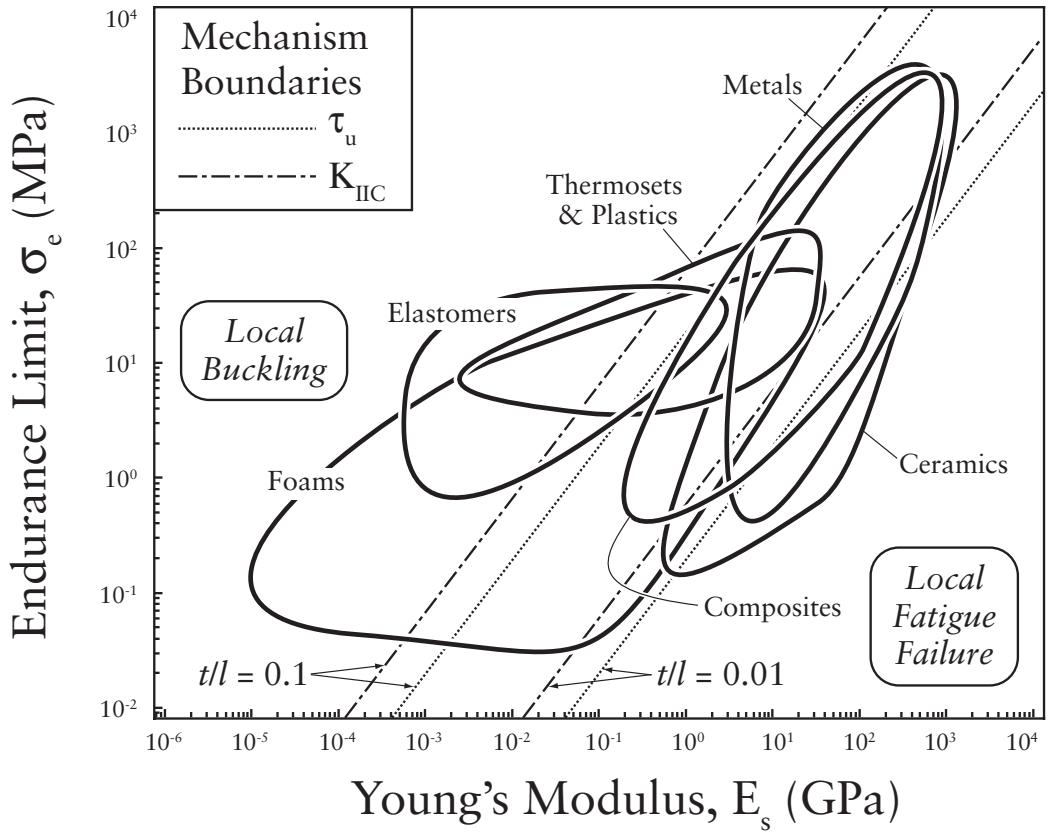

Figure 13. Material-property chart for failure mechanisms dictating the fracture toughness and unnotched strength of a lattice core subjected to shear cyclic loading. Note that $\Pi \equiv \sigma_e l^2 / E_S t^2$.